Pergamon

Geochimica et Cosmochimica Acta, Vol. 66, No. 20, pp. 3549–3562, 2002

0016-7037/02 $22.00 + .00

PII S0016-7037(02)00972-9

Cadmium deposition and mobility in the sediments of an acidic oligotrophic lake

MA. CATALINA ALFARO-DE LA TORRE and ANDRÉ TESSIER*
INRS–Eau, Université du Québec, C.P. 7500, Sainte-Foy, Québec, G1V 4C7, Canada

(*Received May* 30, 2001; *accepted in revised form May* 28, 2002)

Abstract—A dated core from the profoundal zone in a pristine oligotrophic acidic lake was analyzed for Cd as well as for Al, Ca, Fe, Mg, Mn, Pb, Ti and total carbon and nitrogen. Overlying water and porewater samples were also obtained on six occasions at the same site, and yielded vertical profiles of pH and dissolved Cd, Ca, Fe, Mg, Mn, sulfide, SO_4^{-2}, organic and inorganic carbon concentrations. These extensive porewater and sediment geochemical data were used, together with information on infaunal benthos, to decipher the sedimentary record of Cd contamination. Depth variation of sediment Ca concentrations indicate that the lake suffered from progressive acidification starting about 1950. The present-day accumulation rate of Cd ($J_{acc}^{Cd} = 5.4 \pm 0.4 \times 10^{-11}$ mol cm^{-2} yr^{-1}) in the sediments is the sum of the flux of Cd deposited with settling particles ($J_S^{Cd} = 3.3 \pm 0.2 \times 10^{-11}$ mol cm^{-2} yr^{-1}) and the fluxes of dissolved Cd across the sediment-water interface due to molecular diffusion ($J_D^{Cd} = 1.8 \pm 0.3 \times 10^{-11}$ mol cm^{-2} yr^{-1}), bioturbation ($J_B^{Cd} = 1.1 \pm 0.2 \times 10^{-14}$ mol cm^{-2} yr^{-1}) and bioirrigation ($J_I^{Cd} = 0.27 \pm 0.05 \times 10^{-11}$ mol cm^{-2} yr^{-1}). Biological mixing of the sediments was negligible. The shape of the vertical profile of total Cd concentration with depth in the sediment appears to be determined more by its input history than by post-depositional mobilization and redistribution in the sediment column. *Copyright © 2002 Elsevier Science Ltd*

1. INTRODUCTION

Human activities such as metal mining, smelting and finishing, refuse incineration, burning of fossil fuels, and agriculture have greatly increased the fluxes of trace metals to the aquatic environment (Pacyna et al., 1995). Of particular concern are increases over the past 100 years in atmospheric metal emissions that have resulted in contamination on regional and even global scales following long-range transport and deposition at remote sites. Lake sediments are important sinks for trace metals of atmospheric origin and accordingly record their deposition history. Consistent with this idea is the fact that sediment metal concentrations typically increase from deeper sediments towards the sediment-water interface (Nriagu and Rao, 1987; Gobeil, 1999; Gobeil et al., 1999; Evans et al., 1983). However, the interpretation of such profiles is complex because several processes occur simultaneously that could contribute to their shape.

Processes involved in the transport of trace metals and other sediment constituents to the sediment coring site should be considered when interpreting trace metal concentration profiles. For example, mass accumulation rates of the inorganic or organic matrices of sediments can increase with time due to increased runoff as a consequence of either deforestation, forest fires or other human-mediated changes (Martin et al., 2000); the result of these processes is the dilution of anthropogenic metals in sediments. Furthermore, changes over time in the scavenging of metals in the water column by settling particles and in sediment focussing can be brought about by acidification of the water column or by eutrophication (Norton and Kahl, 1991).

Various complex diagenetic processes can also influence sedimentary trace metal concentration profiles. Diffusion of metal to a sink located below the sediment–water interface can occur if dissolved metal concentrations are higher in the water column than in porewaters (Carignan and Nriagu, 1985; Carignan and Tessier, 1985); this can create subsurface peaks in sedimentary metals that could be erroneously attributed to variations in metal deposition. Trace metals can also be mobilized after their deposition and then either relocalized in the sediment column (Gobeil et al., 1987; Gobeil and Cossa, 1993; McCorkle and Klinkhammer, 1991) or diffuse to the water column (Gobeil et al., 1987; Morfett et al., 1988). Redox reactions of other compounds such as the degradation of labile organic matter and the recycling of Fe and Mn oxyhydroxides (Davison, 1993) in the upper layers of the sediment column can also influence the sediment concentration of a given trace metal. The upper layers of sediments can be mixed by physical processes due to the burrowing and feeding activities of benthic organisms; these mixing processes tend to homogenize metal concentrations in the mixing zone (Matisoff, 1995). Most benthic animals pump oxygenated water through their burrows to satisfy their respiration and feeding needs. This advective transport of fluid enhances the exchange of dissolved metal between the water column and porewaters (Matisoff, 1995); it can also promote redox reactions involving metals and increase mobilization of metals to porewaters (Aller and Yingst, 1978).

The above considerations indicate that the correct interpretation of trace metal concentration profiles in terms of emission chronology calls for a comprehensive set of geochemical and biological data. Despite the evident complexity of the processes, the relative contribution of metals from anthropogenic sources is often inferred solely from sediment metal concentration profiles (Blais et al., 1998; Heyvaert et al., 2000; Wong et al., 1984). Because conclusions drawn from the interpretation of trace metal profiles have serious ecological and economic implications, it is important to carefully examine the assumptions underlying such interpretations. In the present study, we use extensive porewater and sediment geochemical

* Author to whom correspondence should be addressed (atessier@inrs-eau.uquebec.ca).

data as well as information on the infaunal benthos to interpret the Cd concentration profile in a dated core obtained from a pristine oligotrophic lake located on the Canadian Precambrian Shield.

2. STUDY SITE

Lake Tantaré (47°04'N, 71°32'W) is a small (1.1 km^2), headwater, acidic (pH 5.3–5.6), and oligotrophic (*Chl a* 0.2–0.9 nM; total $P < 5$ nM; planktonic primary production of 50 mg C m^{-2} d^{-1}; Hare et al., 1994) lake located in an Ecological Reserve about 40 km northwest of Quebec City, QC, Canada (Fig. 1). This dimictic lake has four basins connected by shallow channels. Our study took place at the deepest site (15 m) in the westernmost basin (Fig. 1), which has the following physical characteristics: volume of 1.08×10^6 m^3, maximum depth of 15 m, mean depth of 7.4 m, and water residence time of 78 d. At the coring site, the sediments support a small density of invertebrates (1690 ± 180 animals m^{-2}), the major taxon being the chironomid *Sergentia coracina* (1080 ± 140 animals m^{-2}) (Hare et al., 1994). Aquatic plants (mainly *Isoetes*) are abundant in the 0 to 7 m zone and algal mats (*Mougeotia*) are present between 7 and 9 m. During stratification periods, $[O_2]$ decreases progressively in the hypolimnion of this basin, but it does not become anoxic. The lake is covered with ice from the beginning of December to early May.

Most of the small drainage basin of L. Tantaré (9.2 km^2) is located within the limits of the Ecological Reserve (Fig. 1) created in 1978 for nature conservation and scientific research. The uninhabitated reserve is accessible only by one narrow road. Being at the southern limit of the Precambrian Laurentide plateau, the watershed has a mixed forest of St. Lawrence Lowlands (maple, yellow birch) and boreal forest (fir, spruce, white birch) species and the soils are mostly humo-ferric podzols (Payette et al., 1990). Selective tree cutting occurred in about 2% of the watershed between 1961 and 1972 (Fig. 1) and no forest fires have been documented since records began in 1940 (J. Fortin, Quebec Ministry of Natural Resources, personal communication). The watershed belongs to the Grenville geological province and is underlain by crystalline metamorphic bedrock of the Precambrian Shield, covered by a thin layer of till (MEQ, 1990). It is characterized by a rough topography with elevation varying between 450 (lake) and 730 m. The mean annual temperature is 3.2 °C and the average (from 1984 to 1994) total annual precipitation is 1015 mm, of which about 435 mm falls as snow (Ouellet and Jones, 1983).

3. METHODS

3.1. Sampling

Sediment, overlying water, and porewaters were sampled from 1997 to 1999. Labware and material for sampling porewater were cleaned in diluted (7–15 % *v*/*v*) HNO_3 and rinsed with ultrapure water (>18 MΩ cm) prior to use.

3.1.1. Sediment cores

Two sediment cores were collected in October 1997 by divers using 9.5 cm internal diameter Plexiglas tubes. Within 2 h, they were extruded and sectioned at 0.5 cm intervals from the sediment surface to 10 cm and at 1 cm intervals from 10 to 20 cm. Core slices were placed in 100 mL plastic vials, kept at 4 °C during their transport to the laboratory, frozen within 3 h and kept frozen until freeze-dried.

3.1.2. Porewaters and overlying water

Acrylic porewater samplers (1 cm vertical resolution peepers, two columns of 4 mL cells) were deployed (three peepers, left in place for 2 weeks) on six occasions (28 August and 6 October 1997, 7 May, 28 May, and 2 July 1998, and 28 May 1999) during the ice-free period to collect porewater and overlying water. Sampling porewaters by this technique and by centrifugation followed by filtration produces similar results (Carignan et al., 1985). Peepers were deaerated with N_2 for a minimum of 15 d prior to filling the cells with ultrapure water and covering them with a membrane (Gelman HT-200; 0.2 μm); they were stored under a N_2 atmosphere again for at least one week to ensure removal of traces of O_2 prior to their placement in lake sediments (Carignan et al., 1994a).

Upon retrieval, peepers were sampled for the measurement of pH and concentrations of Cd, sulfide (ΣS(-II)), SO_4^{2-}, Fe, Mn, Ca, Mg, organic carbon (DOC) and inorganic carbon (ΣCO_2). Samples (1 mL) for [ΣS(-II)] were collected first (within 2 min) with N_2-purged polypropylene syringes and injected through Teflon-lined septa into 2 mL N_2-purged amber vials containing 0.0027 M N,N'-dimethyl-p-phenylenediamine sulfate (Eastman Kodak) and 0.0055 M $FeCl_3$ (40 μL of each). Blanks were prepared in the field by injecting ultrapure water into vials containing the same reactants. Samples and blanks were stored at 4 °C in the dark for their transport to the laboratory. Samples for ΣCO_2 and DOC (1 mL) were collected from the same cells with N_2-purged polypropylene syringes and injected through Teflon-lined septa into 4 mL He-purged and preacidified (40 μL HCl 10%) amber glass vials. Samples (1 mL) for pH were also collected from the same cells with 1 mL plastic syringes and the pH was measured within 10–30 min with a combination microelectrode (Microelectrode Inc., Model MI-710) or semimicroelectrode (VWR, gel filled). The remaining 1 mL of water in the cells was collected for SO_4^{2-} measurement using a Gilson pipette equiped with a plastic tip and injected into prerinsed polypropylene Eppendorf tubes. Samples (3 mL) for Cd and major cations were obtained from cells of the second column by piercing the membrane with a Gilson pipette fitted with an acid-washed plastic tip and injected into prewashed and preacidified (45 μL of 1.5 M HNO_3; Anachemia Environmental grade; final pH <2.5) 4 mL high-density polyethylene (HDPE) vials.

3.2. Analyses

3.2.1. Sediments

Freeze-dried sediment subsamples from one core were completely digested with HF, HNO_3, and $HClO_4$ in Teflon beakers. Concentrations of Al, Ca, Fe, Mg, Mn, and Ti were measured by inductively coupled plasma optical emission spectrometry (ICP–OES; Vista AX CCD) and those of Cd and Pb by graphite furnace atomic absorption spectrometry (GFAAS; Perkin-Elmer SIMAA 6000; Zeeman correction). Certified reference materials Mess-2 and PACS-2 from the National Research

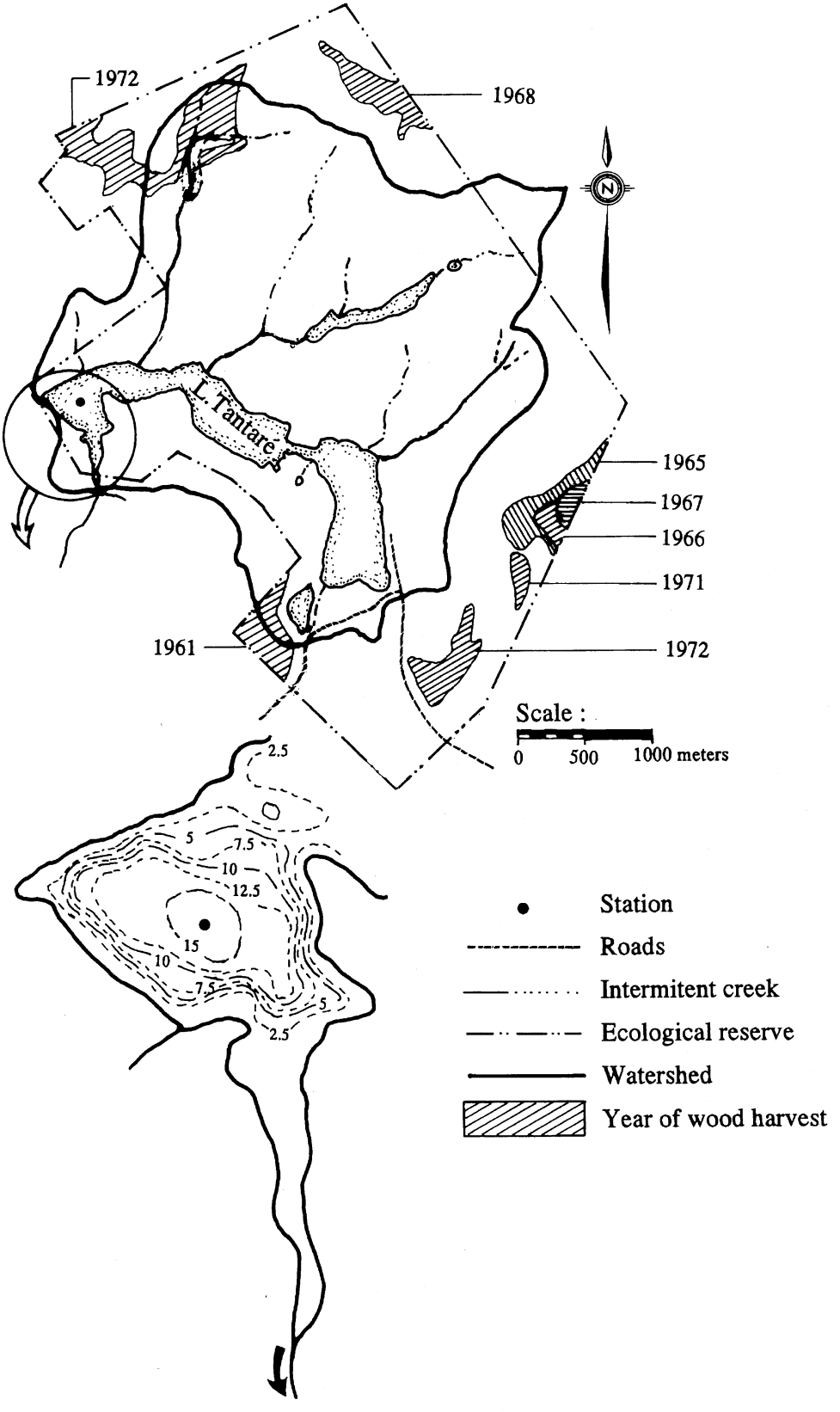

Fig. 1. Map of Tantaré Ecological Reserve and of the L. Tantaré drainage basin, including the access road, the areas where (and dates when) wood harvesting occurred, and the bathymetry (isolines are in meters) of the westernmost lake basin where sampling occurred (sampling site, ●).

Council of Canada (NRCC) and SRM 2704 from the National Institute of Standards (NIST) were regularly digested and analyses of Cd and Pb were within 8% and 10% of the certified values, respectively. Precision, expressed as the coefficient of variation for the digestion of replicate aliquots of a certified standard, was the following: 4.5% for Fe ($n = 13$); 3.7% for Mn ($n = 13$); 1.5% for Ca ($n = 4$); 1.3% for Mg ($n = 4$); 1.4% for Al ($n = 4$); 2.1% for Ti ($n = 4$); 5.7% for Cd ($n = 10$); and 7.3% for Pb ($n = 6$). Total organic carbon (TOC) and total nitrogen (TN) were measured using a NCS analyzer (Carlo Erba Model NA-1500); precision for replicate analyses ($n = 4$) of a certified reference (Mess-2) was 1.1% for TOC and 6.9% for TN.

Freeze-dried samples from a second core were placed in sealed Al vials. After at least 1 month to allow for secular equilibrium of ^{222}Rn and ^{214}Pb with ^{226}Ra, ^{137}Cs, ^{241}Am, and ^{210}Pb were measured by Compton-suppressed gamma spectrometry and corrected for sample geometry and self-absorption (Canberra equipment; Carignan et al., 1994b). Counting efficiencies were determined by labelling dry sediment samples (bulk densities from 0.5 to 1.6 g cm^{-3}) with standard solutions (Amersham) of mixed nuclides (QCY.48), ^{210}Pb (RBZ.44), and ^{226}Ra (RAY.44). Measurements were made at 46.7 keV (^{210}Pb), 59.5 keV (^{241}Am), 343 keV (^{214}Pb), and 662 keV (^{137}Cs) and unsupported ^{210}Pb activity (^{210}Pb$_{un}$) was obtained by subtracting, from total ^{210}Pb activity, the ^{226}Ra-supported ^{210}Pb activity as measured by ^{214}Pb activity at secular equilibrium.

We determined the net dry mass of material delivered to the sediment (m_n; g per sediment interval) as follows:

$$m_n = m_t - m_{Fe}, \quad (1)$$

where m_t and m_{Fe} are the total dry mass and that of excess Fe oxyhydroxides, respectively; "excess Fe" corresponds to the enrichment of Fe within a few centimeters of the sediment–water interface, relative to Fe concentrations measured at greater depths. This enrichment is due to Fe recycling (see Sect. 5.1 below). Diagenetically formed Fe oxyhydroxide temporarily dilutes the concentrations of all elements supplied to the sediment from the water column. Consequently, m_n values were used to calculate element (including radiometal) concentrations as well as cumulative mass of sediments (m_c). In using Eqn. 1, we assumed that excess Fe was in the form of $Fe(OH)_3(s)$. This correction to the sediment mass amounts to a maximum of 12% at the sediment–water interface and becomes vanishly small below about 5 cm.

3.2.2. Porewaters

The detection limits (DL) are defined as 2.5 times the standard deviation of a sample of low concentration. Cadmium was measured by GFAAS (DL of 0.04 nM), using a multiple injection technique due to the low Cd concentrations. Blanks and certified samples (1643d from NIST, and SLRS-3 from NRCC) were used on a regular basis and analyses of Cd were within 15% of the certified values. Major cations (Ca, Mg, Na, K) and higher Fe and Mn concentrations were determined by ICP–OES; low concentrations of Fe (<1 μM) and Mn (<0.5 μM) were measured by GFAAS (DL of 7 nM for both Mn and Fe). Precision, expressed as the coefficient of variation for replicate analyses of a certified standard, was the following: 3.5% for Fe ($n = 11$); 1.7% for Mn ($n = 11$); 2.5% for Ca ($n = 13$); 2.7% for Mg ($n = 13$); 3.0% for Na ($n = 13$); 11% for K ($n = 11$); and 22% for Cd ($n = 20$). Sulfide concentrations [ΣS(-II)] were measured, within 4–6 h of collection, by colorimetry (660 nm; Cline, 1969) in a 2 cm flowcell (Technicon Auto Analyser II; DL of 4 nM). Dissolved inorganic carbon was measured by gas chromatography (Perkin-Elmer Sigma 600; Porapak-Q column; DL of 0.08 mM), DOC with a carbon analyzer (Shimadzu TOC-5000A; DL of 0.02 mM), and sulfate by ion chromatography (Dionex IONPAC AS14 Suppressed Conductivity ASRS-II; DL of 0.12 μM).

4. RESULTS

4.1. Chronology of Sedimentation

Figure 2a displays the plots of unsupported ^{210}Pb (^{210}Pb$_{un}$), ^{137}Cs, and ^{241}Am activities vs. depth; it shows that the concentration of ^{210}Pb$_{un}$ decreases progressively from 1.7 Bq g^{-1} at a depth of 0.25 cm to levels close to zero at depths below 13.5 cm. There is close agreement between ^{210}Pb$_{un}$ activities from this study and those obtained at the same site 13 years earlier by Carignan and Tessier (1985) once adjusted to our sampling date, even though different methods were used to obtain ^{210}Pb$_{un}$ (Fig. 2b). Carignan and Tessier (1985) obtained ^{210}Pb$_{un}$ by measuring its decay product, ^{210}Po (Eakins and Morrison, 1978); that method, contrary to the one used in the present study, assumes that the correction for supported ^{210}Pb is constant at all depths. To establish the ^{210}Pb chronology, we used the SCFCS model (Heyvaert et al., 2000; Robbins, 1978), which is a stepwise application of the CFCS (constant flux constant sedimentation) model. Figure 2b suggests that a higher deposition event occurred between 4 cm and 5 cm, presumably an episodic sediment slumping, which is common in lakes (Binford, 1990; Robbins and Herche, 1993). In agreement with this interpretation, the slopes of the segments in the log ^{210}Pb$_{un}$ profile above (from 0.25 to 3.75 cm) and below (from 5.25 to 8.75 cm) the 4–5 cm interval were not statistically different (t-test); similar observations resulted from the log ^{210}Pb$_{un}$ vs. m_c plot. As a consequence we pooled all the log ^{210}Pb$_{un}$ data from 0.25 to 8.25 cm (except those for the 4–5 cm interval) to obtain single values of mass accumulation rate ($R_m = 7.34 \pm 0.13$ mg cm^{-2} yr^{-1}; $r^2 = 0.996$; $n = 16$) and sedimentation rate ($R_s = 0.114 \pm 0.002$ cm yr^{-1}; $r^2 = 0.996$; $n = 16$). In contrast, the slopes of log ^{210}Pb$_{un}$ vs. depth or m_c obtained for the 8.75 to 13.5 cm depth interval were statistically different from those obtained for the upper part of the ^{210}Pb$_{un}$ profiles; they yielded $R_m = 3.84 \pm 0.32$ mg cm^{-2} yr^{-1} ($r^2 = 0.96$; $n = 8$) and $R_s = 0.072 \pm 0.006$ cm yr^{-1} ($r^2 = 0.96$; $n = 8$). Figure 2b shows that the predicted ^{210}Pb$_{un}$ profile (regression lines) compares well with the observations (open circles). As shown below (Sect. 5.1 and Fig. 4), the change in R_m (or R_s) is consistent with changes in the composition of the sediment matrix that occurred at approximately the same depth. Dates were obtained by multiplying R_m by the m_c value at mid-depth of a sediment interval and error propagation was used to estimate dating errors (Binford, 1990). Errors, expressed as 95% confidence intervals, increased from 0.04 yr at the top of the core, to 0.6 yr at 4 cm, 2.5 yr at 8.75 cm, and 9.2 yr at the

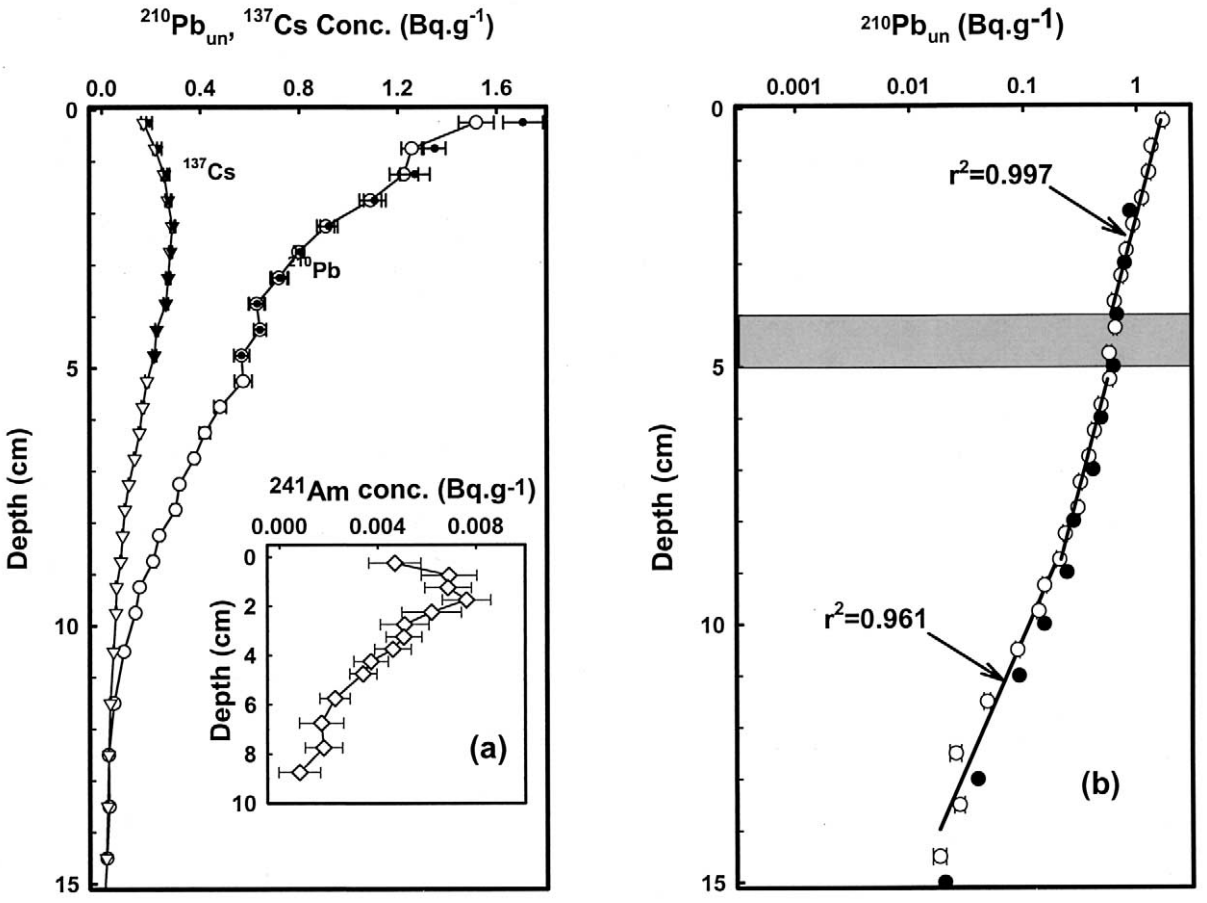

Fig. 2. Downcore $^{210}Pb_{un}$, ^{137}Cs, and ^{241}Am concentration profiles at the deepest site of the westernmost basin of L. Tantaré (a), and log of $^{210}Pb_{un}$ activity vs. depth profile (b). ● symbols in (a) are for data corrected for diagenetic Fe; ● in (b) is for $^{210}Pb_{un}$ data from Carignan and Tessier (1985) adjusted for our sampling date and corrected for diagenetic Fe. The shaded area indicates the depth at which a rapid deposition due to sediment slumping probably occurred. Experimental data are represented by symbols with counting error (±SE); the lines in (b) represent prediction with the SCFCS model.

bottom of the datable interval (14.5 cm). It should be noted that the shift that shows at 4–5 cm in the log ^{210}Pb vs. depth profile (Fig 2b) is not explained by the low uncertainty in the date at this depth.

Dates using the SCFCS ^{210}Pb geochronology model are inconsistent with known events in North America involving ^{137}Cs and ^{241}Am emissions, i.e., initial input about 1953 and maximum fallout from nuclear weapons in 1963. The peaks of ^{137}Cs and ^{241}Am (Fig. 2a) are shallower and activities of the two radionuclides occurred deeper than predicted by the ^{210}Pb model. The occurrence of ^{137}Cs and ^{241}Am activities at much greater depths (~10 and 8 cm, respectively) than expected (about 5 cm) is an indication of postdepositional mobility; this contention is supported by the absence of sharp peaks in the two profiles, as expected from the known input history (Appleby et al., 1991). The remobilization of ^{137}Cs has been reported for a large number of lakes including Canadian Shield lakes (Anderson et al., 1987; Davis et al., 1984), and the upward shift of the peak has been attributed to the redistribution of ^{137}Cs initially incorporated in epilimnetic sediments; this tracer has a low affinity for settling particles and tends to react with littoral sediments. Winnowing of fine littoral sediments and their transport to deeper parts of the lake provides an additional supply of ^{137}Cs to the deeper site and can delay its peak (Anderson et al., 1987). Retardation of the peak can also be caused by recycling of Cs in the catchment (Davis et al., 1984). Crusius and Anderson (1995) also showed that Pu (^{241}Am is the daughter product of ^{241}Pu) is mobile in Precambrian Shield lake sediments, although to a lesser extent than Cs. The upward shift of ^{241}Am is difficult to explain since Pu is reputed to be delivered more rapidly than Cs to the deep sediments (Crusius and Anderson, 1995).

Stable lead can also be used as a stratigraphic marker to corroborate predicted ^{210}Pb dates. In North America, anthropogenic Pb has been emitted to the atmosphere mainly by combustion of coal and leaded gasoline as well as by smelting activities (Edgington and Robbins, 1976; Nriagu, 1990). However, the occurrence of stable Pb events has not been as securely dated as those of ^{137}Cs and ^{241}Am since long-term monitoring of Pb in precipitation or in the atmosphere has not been performed. Sediment lead concentration profiles are often characterized by a well defined peak attributed to the phasing out of leaded gasoline in the 1970s; suggested dates for the occurrence of this event vary between 1973 and 1975 for

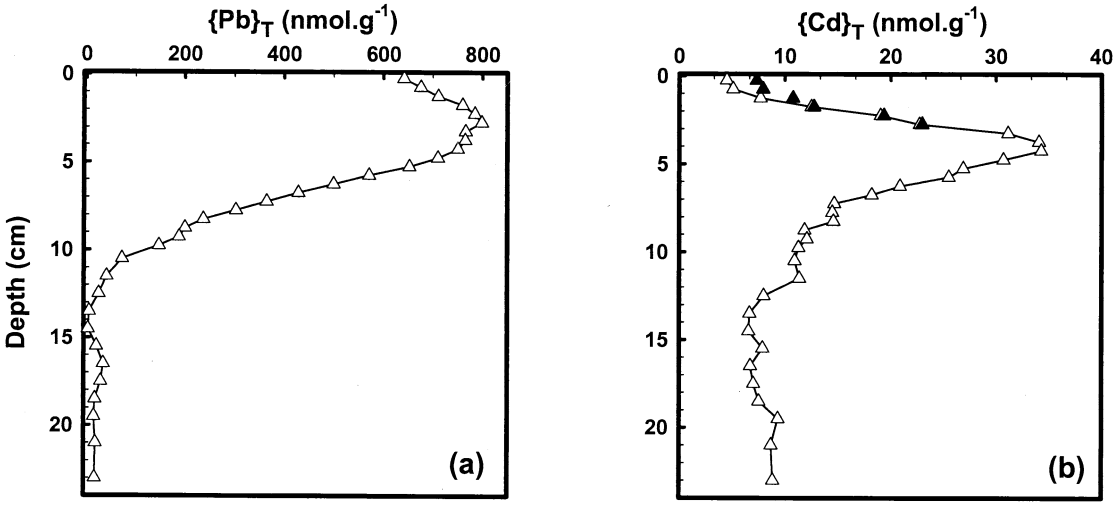

Fig. 3. Depth concentration profiles of Pb (a) and Cd (b) in a sediment core collected at the deepest site of the westernmost basin of L. Tantaré. The filled symbols indicate the expected {Cd} values when the sediment will be buried below 8 cm depth.

Canada (SRC, 1985; Nriagu, 1990), and between 1972 and 1975 for the USA (Blais et al., 1998; Eisenreich et al., 1986; Heyvaert et al., 2000; US EPA, 1995; Nriagu, 1990). Figure 3a shows a peak in total Pb at a depth of 2.75 cm which corresponds to a predicted date of 1976 ± 1 (±95% CI) by the SCFCS model.

4.2. Solid Phase and Dissolved Concentration Profiles

The depth profiles of sedimentary Pb and Cd concentrations are displayed in Figure 3, and those of Al, Ca, Fe, Mg, Mn, Ti, organic carbon (C_{org}) and total nitrogen (N_T) in Fig. 4. The molar ratio C_{org}:N is high and relatively constant with depth (mean value ±SD = 15.5 ± 0.5; Fig. 4g). High C/N ratios (e.g., 11–15; Wong et al., 1984) have been reported for Canadian Shield lakes. This ratio in L. Tantaré is close to that of humic substances (17.5; Buffle, 1988) and higher than the C/N Redfield ratio for phytoplankton (6.67; Stumm and Morgan, 1996) or than the ratios for lakes where organic matter is mainly autochthonous (Hamilton-Taylor et al., 1984; Sigg et al., 1987). Also, C_{org} in the settling particles of L. Tantaré is not correlated with primary production nor with deposition rate of settling particles (Alfaro–De la Torre, unpublished results). Thus, it is reasonable to assume that most of the sediment C_{org} in L. Tantaré is from allochtonous humic substances (HS). Assuming that HS is 50% C (Buffle, 1988), we calculated the concentrations of Al, Ca, Fe, Mg, Mn, and Ti in the inorganic matrix; this is equivalent to measuring the concentration of these elements after the combustion of organic matter. Thus, Figure 4 displays concentrations of element "*i*" expressed with respect to the dry weight of both total sediment ($\{i\}_T$) and the inorganic fraction ($\{i\}_{in}$). An example of porewater pH and SO_4^{2-}, ΣS(-II), Ca, Mg, Fe, and Mn concentration profiles measured in July 1998 is shown in Figure 5; profiles obtained at other dates are discussed below (Sect. 5.1). Cadmium concentration profiles obtained for all sampling dates are displayed in Figure 6.

5. DISCUSSION

5.1. Sedimentary Record of Changes in Sediment Composition

Sediment Al, Ca, Fe, Mg, Mn, and Ti originate from erosion of the drainage basin and from atmospheric deposition on the lake surface or in the catchment; an additional source for C_{org} and N_T is primary production in the water column. The concentration profiles of these elements (Fig. 4) depend not only on the input history, but also on diagenetic reactions such as the redox-driven migration of Fe. The Fe profile (Fig. 4b) exhibits higher Fe concentrations from the sediment–water interface to 2.5 cm below than at greater depths as a consequence of the reduction of reactive Fe(III) in the lower sediment strata, upward diffusion of porewater Fe(II), and its oxidation and fixation in the top oxic sediment as lepidocrocite and other poorly crystallized Fe(III) solids (Fortin et al., 1993). Dissolved [Fe] profiles (Fig. 5a and profiles not shown for other sampling dates) support this iron cycling mechanism. The effect of this diagenetic process is to dilute the sediment matrix by up to 12% in the surface layer of sediments if we assume that the authigenic solid is $Fe(OH)_3$(s). Thus, it is difficult to understand the long-term changes in geochemical variables by considering only the element concentration profiles individually because they are dependent upon those of other elements. Normalization with respect to the concentration of a relatively inert element (e.g., Ti or Al) and expression of the data as element accumulation rates (fluxes) are useful complements to the interpretation.

The depth profile of $\{Al\}_{in}$ (Fig. 4e) indicates that the proportion of Al remained relatively constant in the inorganic matrix with the exception of a peak at 11.5 cm observed also in Figure 4 for all the components of the inorganic matrix that we measured. The profiles of $\{Mn\}_{in}$, $\{Ca\}_{in}$, $\{Mg\}_{in}$, and $\{Ti\}_{in}$ display a trend similar to that of $\{Al\}_{in}$ from 8.75 cm downward (Fig. 4a, 4c, 4d and 4f); however, the upper part of their

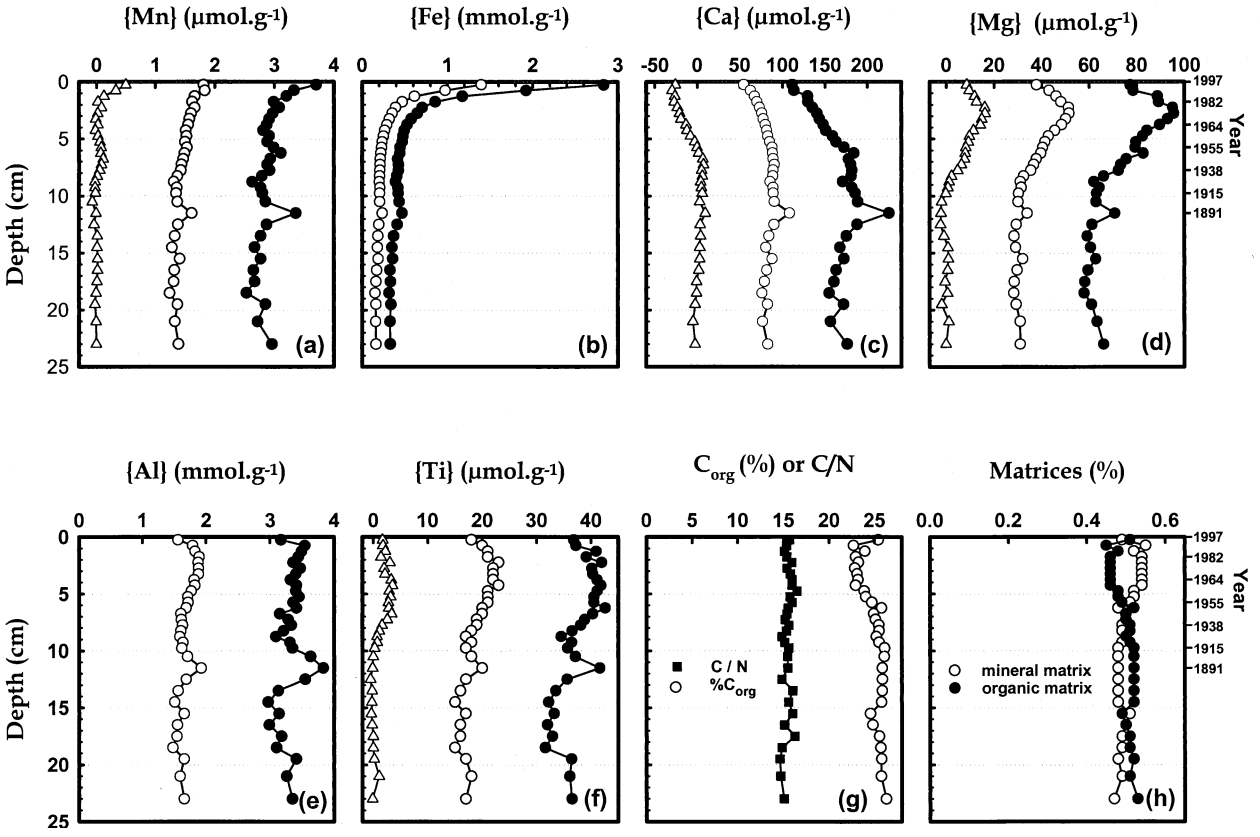

Fig. 4. Depth concentration profiles of Mn (a), Fe (b), Ca (c), Mg (d), Al (e), Ti (f), organic carbon (g), and organic and inorganic matrices (h) in a sediment core collected at the deepest site of the westernmost basin of L. Tantaré. For (a)–(f), the various symbols indicate concentrations expressed either as a function of the total sediment ($\{i\}_T$; ○) or as a function of the inorganic matrix ($\{i\}_{in}$; ●), and anthropogenic contribution ($\{i\}_x^a$; △); for (g) and (h), symbol meaning is indicated on the panels. The dates indicated are derived from the ^{210}Pb SCFCS model. Propagation of errors gives the following precision (±SD in μmol g^{-1}) on $\{i\}_{in}$ and $\{i\}_x^a$, respectively, for Mn (0.1 and 0.1), Fe (0.03 and 20), Ca (3.0 and 5.8), Mg (1.2 and 2.1), and Ti (0.9 and 1.3).

profiles differs from that of $\{Al\}_{in}$. If sedimentary Al is assumed to originate mainly from erosion of the catchment, then the increase in $\{Ti\}_{in}$, $\{Mn\}_{in}$, and $\{Mg\}_{in}$ relative to $\{Al\}_{in}$ indicates another source for these elements which is probably of anthropogenic origin. The anthropogenic contribution ($\{i\}_x^a$) to the concentration of an element i at depth x ($\{i\}_x$) can be estimated as follows (Norton and Kahl, 1991):

$$\{i\}_x^a = \{i\}_x - \{i\}_b \cdot \frac{\{Al\}_x}{\{Al\}_b}, \qquad (2)$$

where the background values for species i and Al, identified by the index b, are taken as the average values from depths 13.5 cm downward (<1850); these concentrations are assumed to have been contributed only from the geology. In this calculation, it is also assumed that all the Al is from erosion of the catchment, and that the geologic component of element i was contributed at any depth in constant proportion to Al. We choose Al rather than Ti (Norton and Kahl, 1991) to estimate the geologic contributions because the depth concentration profiles of Ti (Fig. 4f) suggest an anthropogenic contribution, which does not seem to be the case for Al (Fig. 4e).

The concentrations of anthropogenic Mg and Ti, as calculated with Eqn. 2, are important (Figs. 4d and 4f) and began in about 1905 ± 7 (depth of about 9.5 cm). The fluxes of atmospheric Ti (0.8–27 nmol cm^{-2} yr^{-1}) and Mg (2–135 nmol cm^{-2} yr^{-1}), calculated as the product of R_m and $\{i\}_x^a$, fall within the range of depositional fluxes of these elements reported for dated ombrotrophic peat bogs (4–40 nmol cm^{-2} yr^{-1} for Ti and 80–700 nmol cm^{-2} yr^{-1} for Mg; Norton et al., 1991; Pakarinen et al., 1983). These bogs are reputed to receive their inorganic matrix components from atmospheric deposition alone. The same depth (9.5 cm) corresponds also to the onset of a decrease in C_{org} (Fig. 4g) and approximately to the change observed in sedimentation rate (Fig. 2b). All these changes may be related to the installation (~1918) of the Canadian Forces Base in Valcartier which borders the reserve to the east and to the settlement and development of small villages close to the ecological reserve (Shannon, 17 km southeast; Valcartier, 13 km southeast; Tewkesbury, 9 km east). The upward increase of $\{Mn\}^a$ in the top 1.75 cm (Fig. 4a) is due to diagenetic remobilization by a redox process similar to that of Fe rather than to an anthropogenic contribution. Profiles of $\{Ca\}_{in}$ (Fig. 4c) show a sharp decline starting about 1944 ± 2 due to progressive acidification of the ecosystem (Norton and Kahl, 1987).

Another notable feature in Figure 4 is the peak at 11.5 cm

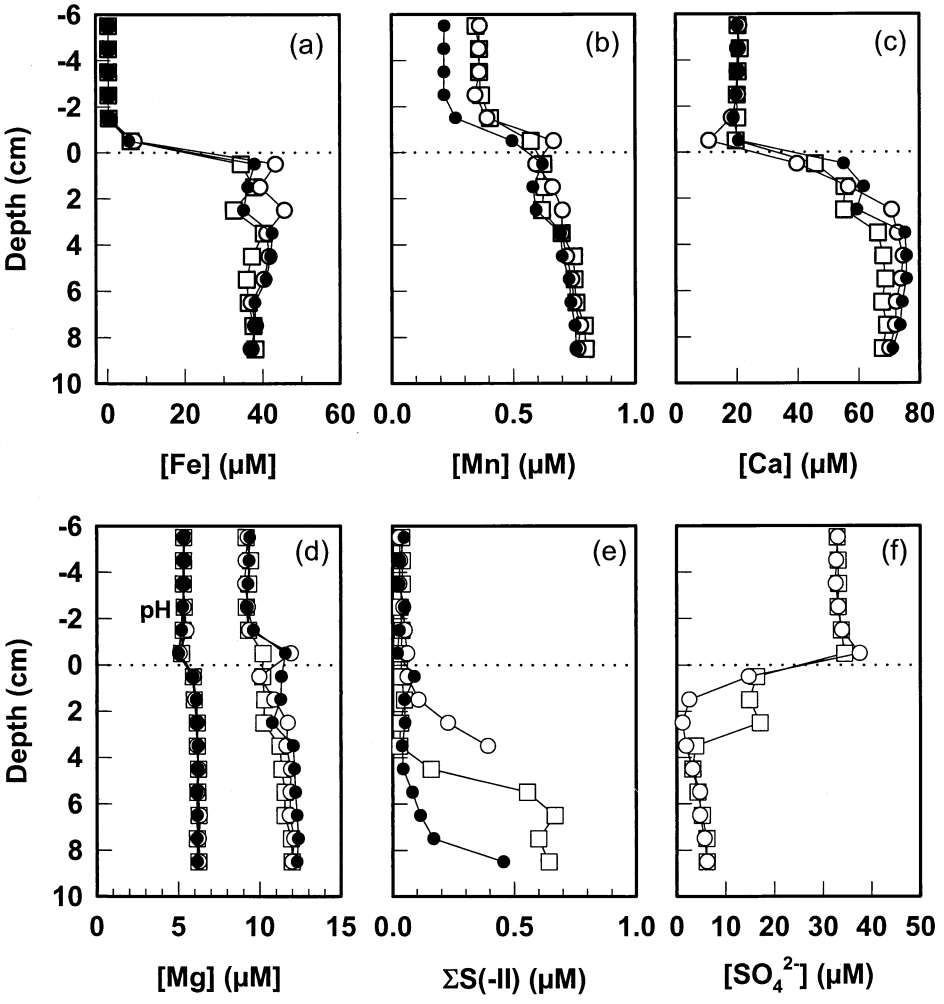

Fig. 5. Porewater iron (a), manganese (b), calcium (c), magnesium and pH (d), sulfide (e), and sulfate (f) concentration profiles obtained in July 1998 at the deepest site of the westernmost basin of L. Tantaré. The horizontal broken lines indicate the sediment–water interface. The various symbols are for replicate profiles.

(1879 ± 13) for Al, Ca, Fe, Mg, Mn, and Ti. This peak also appears in the Cd profile (Fig. 3b), but not in those of the inorganic and organic matrices (Fig. 4h). The processes responsible for these variations in concentrations is unknown.

5.2. Sedimentary Profile of Cadmium

The sediment Cd concentration ($\{Cd\}_T$) increases progressively from a background value of 7.7 ± 1.1 nmol g^{-1} (below 13.5 cm) to a maximum of 34.3 nmol g^{-1} at a sediment depth of 4.25 cm and then decreases to a lower than background value of 4.5 nmol g^{-1} at the sediment–water interface (Fig. 3b). The background value of $\{Cd\}_T$ is much higher than in the upper continental crust (0.9 nmol g^{-1}; Wedepohl, 1995); however, it is in the range reported for the deepest sites of lakes on the Canadian Shield (3.5–13.4 nmol g^{-1}; Evans et al., 1983) and for lakes of northern Wisconsin (5.9–13.6 nmol g^{-1}; Powell et al., 2000). Maximum $\{Cd\}_T$ divided by the background $\{Cd\}_T$ is 4.5, in the range of values reported for the deepest site of Canadian Shield lakes (2.4–6.5; Evans et al., 1983). Given the history of the L. Tantaré watershed, sedimentary Cd in this lake originates mainly from atmospheric deposition and natural erosion and weathering. The maximum enrichment factor (EF) defined as $EF = [\{Cd\}_T/\{Al\}_T]_{sample}/[\{Cd\}/\{Al\}]_{crust}$ is 60; such a high EF value implies a strong atmospheric component. Cadmium is emitted to the atmosphere by both natural and anthropogenic sources; soil particulates due to wind erosion represent ~50% of the total natural emissions in Canada (Richardson, 2000), whereas anthropogenic sources include the combustion of fossil fuels, nonferrous metal production, steel and iron manufacturing, and the incineration of refuse (Pacyna et al., 1995).

The rate of cadmium accumulation in the sediments (J_{acc}^{Cd}) is the sum of various Cd fluxes to the sediments occurring simultaneously,

$$J_{acc}^{Cd} = J_S^{Cd} + J_D^{Cd} + J_B^{Cd} + J_I^{Cd}, \quad (3)$$

where the subscripts *S*, *D*, *B*, and *I* refer to net deposition with settling particles, molecular diffusion, bioturbation, and irrigation, respectively; the last three fluxes involve the transport of

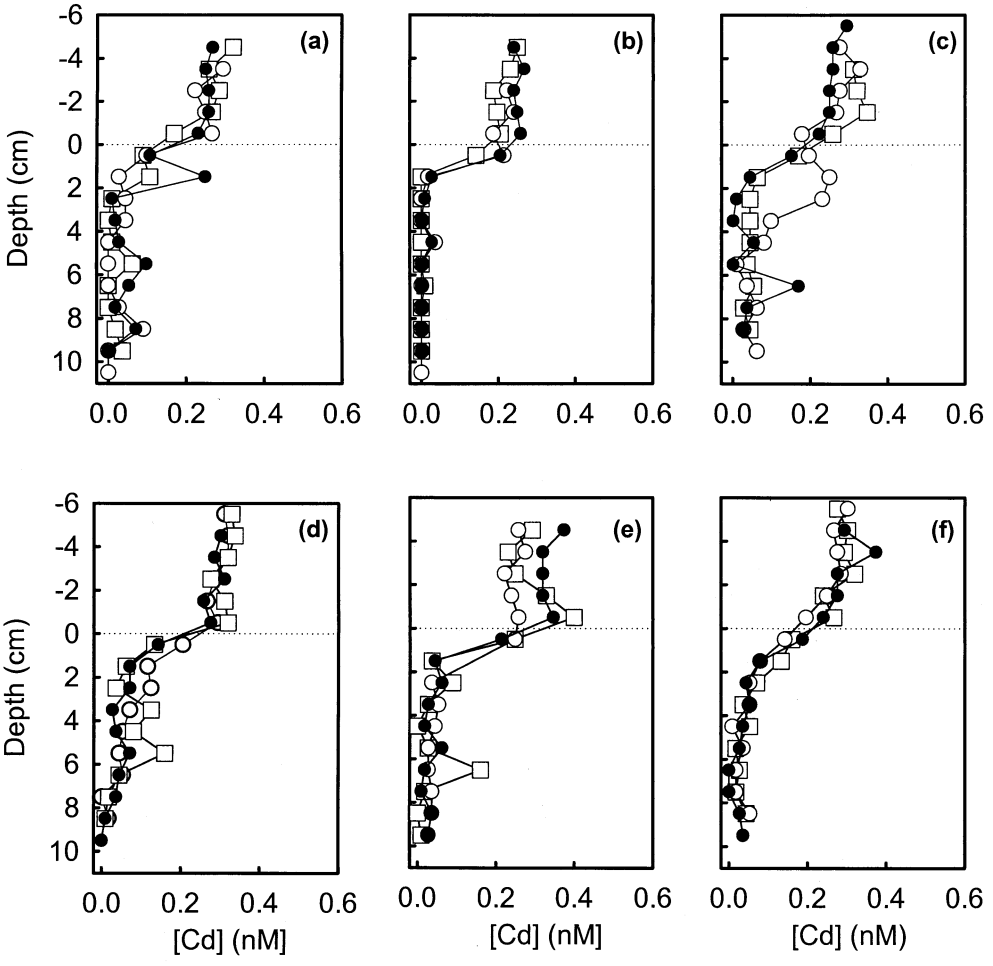

Fig. 6. Porewater Cd concentration profiles obtained in September 1997 (a), November 1997 (b), May 1998 (c), June 1998 (d), July 1998 (e), and June 1999 (f) at the deepest site of the westernmost basin of L. Tantaré. The horizontal broken lines indicate the sediment–water interface. The various symbols are for replicate profiles.

dissolved Cd across the sediment–water interface and its fixation in the sediment. We examine below the contribution of these various Cd fluxes, as well as biological mixing of solids and Cd remobilization in porewaters, in shaping the $\{Cd\}_T$-depth profile.

5.2.1. *Bioturbation (biodiffusion) of solid Cd*

Bioturbation can occur in the upper few cm of the sediment column (mixing zone); it tends to homogenize the sediments, spread metal pulses, and shift concentration maxima to deeper sediment layers (Guinasso and Schink, 1975). The magnitude of these effects increases with the intensity of bioturbation. Biological mixing of solids can be considered as a random process and treated as diffusion; according to this model, the biodiffusional flux of solid Cd, J_b^{Cd}, can be calculated as (Berner, 1980)

$$J_b^{Cd} = -D_B \frac{d(Cd)}{dx}, \quad (4)$$

where D_B is the biodiffusion coefficient ($cm^2\ yr^{-1}$) and $d(Cd)/dx$ is the concentration gradient of solid Cd per unit volume of total sediment, i.e., comprising solids and water. The main problem for calculating accurate J_b values with Eqn. 4 rests on the selection of a D_B value that is characteristic of the site under study.

To our knowledge, no values of D_B have been reported for *Sergentia coracina*, the major taxon at our coring site (Sect. 2); this animal lives in tubes and feeds on sediments (Coffman and Ferrington, 1996). However, Matisoff and Wang (2000) have determined, in laboratory experiments, values of D_B for two genera of Chironomidae: *Coelotanypus* sp. ($D_B = 7 \times 10^{-6}$ $cm^2\ yr^{-1}$ per individual) and *Chironomus* sp. ($D_B = 63 \times 10^{-6}$ $cm^2\ yr^{-1}$ per individual). *Coelotanypus* sp. is a burrowing predator whereas *Chironomus* sp. is a burrowing sediment feeder (Coffman and Ferrington, 1996). Substituting the two values of D_B multiplied by the *in situ* population density of *S. coracina* and the $d(Cd)/dx$ value in the 0–1 cm layer of sediments (7×10^{-11} mol cm^{-4}) into Eqn. 4, we predict that the values of J_b^{Cd} should lie between 0.05 and 0.45×10^{-11} mol $cm^{-2}\ yr^{-1}$. These estimated J_b^{Cd} values are probably maximum figures since (i) D_B values were measured by Matisoff and

Wang (2000) at a higher temperature (12 °C) than our field temperature (4 °C) and D_B increases by about a factor of 2 with a 10 °C increase in temperature (Matisoff and Wang, 2000); (ii) the values of D_B were obtained in short-term experiments (~30 d) compared to the lifetime of the organisms in the field (≥1 yr; Tokeshi, 1995), which tends to overestimate the D_B value since the animals are more active when they have to construct their burrow than later, when they simply live in it. Despite our probable overestimation of J_b^{Cd}, the value that we obtain on this basis ($0.05–0.45 \times 10^{-11}$ mol cm^{-2} yr^{-1}) is still much lower than the value of J_{acc}^{Cd} (5.4×10^{-11} mol cm^{-2} yr^{-1}; see Sect. 5.2.5), which suggests that biological mixing should minimally affect the $\{Cd\}_T$-depth profile.

The relative importance of the biological mixing of solids can also be evaluated from the work of Guinasso and Schink (1975) who have described bioturbation in terms of a time-dependent diffusion model that involves the biodiffusion coefficient (D_B), the thickness of the mixing zone (L; cm) and the sedimentation rate (R_s; cm yr^{-1}). Their model predicts that the importance of biological mixing in shaping the peak of a conservative contaminant depends on the dimensionless mixing parameter ($G = D_B/(L \cdot R_s)$); they have established that for $G \geq 10$, the mixed layer becomes homogeneous and that for $G \leq 0.1$, negligible mixing takes place before the sediments are definitely buried. We estimate that the value of G at our coring site should fall in the range from 0.007 to 0.060 based on the following assumptions: (i) $L = 10$ cm (according to Matisoff and Wang (2000), chironomid larvae construct burrows to about 10 cm); (ii) the values of $D_B = 7$ and 63×10^{-6} cm^2 yr^{-1} per individual determined by Matisoff and Wang (2000) are valid for *Sergentia coracina*; and (iii) $R_s = 0.114$ cm yr^{-1}, as determined from our ^{210}Pb dating. Our range of estimated G values suggests negligible mixing.

The two rough calculations described above (J_b^{Cd} and G) suggest that the biological mixing of solids should have a negligible effect on the shape of the $\{Cd\}_T$-depth profile. This contention is also supported by several observations: (i) Figure 4b shows very steep $\{Fe\}_T$ and $\{Fe\}_{in}$ gradients just below the sediment–water interface that are consistent with an insignificant mixing of sediments; (ii) the ^{137}Cs and ^{241}Am peaks (Sect. 4.1) show an upward rather than a downward shift as predicted from biological mixing; (iii) the $^{210}Pb_{un}$ profiles (Figs. 2a and 2b) do not show any evidence of a mixing zone. Measurements of ^{210}Pb on a core obtained 13 years earlier suggested a mixing zone of about 5 cm at this site (Carignan and Tessier, 1985; see also Fig. 2b); however, further accumulation of sediments over the last 13 years (Fig. 2) and the above discussion contradicts this contention.

5.2.2. *Cd remobilization and redistribution in the sediment column*

Chironomids irrigate their burrows with oxygenated overlying water by undulating their body to satisfy their respiration and feeding requirements (Matisoff, 1995); Cd present in the irrigation water can diffuse from the burrows to the adjacent sediments where it can be immobilized. Since [Cd] is greater in overlying water than in porewater (Fig. 6), the irrigation activity would lead to an increase in porewater [Cd] of the irrigated sediment layers provided that the rate of Cd fixation to the sediments is not faster than its transport to the porewater as a result of irrigation. The importance of the porewater [Cd] increase due to bioirrigation would also depend on factors including abundance, size, and activity of the animals. Cadmium in L. Tantaré sediments is probably fixed in the sediments as a sulfide phase since fixation occurs in the zone where SO_4^{2-} is reduced (Fig. 5f) and dissolved sulfide is present (Fig. 5e). Thermodynamic calculations performed with the computer code WHAM (Tipping, 1994) using porewater data from depths where ΣS(-II) and [Cd] were both above detection limits indicate oversaturation (by 0.5 to 2.2 orders of magnitude) of the porewaters with respect to CdS(s) and suggest that the precipitation of CdS(s) is not instantaneous. Irrigation of burrows with oxygenated overlying water oxidizes material (sulfide, organic matter) to which Cd was bound; such a mobilization of Cd could also contribute to a build-up of Cd in the porewaters.

Visual inspection of Figure 6 indicates that an increase in porewater [Cd] occurs seasonally at our study site. The profiles obtained in November (Fig. 6b) show a sharp decrease in $[Cd]_T$ from 0.3 nM in the overlying water to ≤0.04 nM at 1.5 cm below the sediment–water interface and downward; in contrast, the profiles obtained in May to September (Figs. 6a, 6c, 6d, 6e, 6f) show higher porewater [Cd] than those of November down to 7–8 cm depth, which is a reasonable irrigation depth for chironomids. We hypothesize that the seasonal change in porewater [Cd] shown in Figure 6 is due to a variation in the bioirrigation activity of *S. coracina*. In November, the animals may undergo diapause (inactivity and growth arrest), a condition that occurs widely among chironomid species and which can be driven by factors such as photoperiod and food abundance (Tokeshi, 1995). In contrast, the greater availability of food from May to September would promote increased irrigation activity and lead to a build-up of Cd in porewaters. A few [Cd] peaks below the sediment–water interface indicate local pumping of the overlying water or remobilization due to oxidation of Cd-bearing solids; in particular, one [Cd] porewater profile (empty circles in Fig. 6c) shows a wide Cd subsurface peak indicative of such processes.

Mobilization of Cd to the porewater leads to a post-depositional redistribution of solid Cd within the sediment column. In an effort to examine whether this process affects significantly or not the $\{Cd\}_T$-depth profile (Fig. 3b), we calculated, at the depths where Cd peaks showed in the porewaters, the diffusive flux of Cd with Fick's equation:

$$J_D^{Cd} = \phi D_S \frac{d[Cd]}{dx}, \quad (5)$$

where ϕ is porosity (0.94); D_S is the effective diffusion coefficient of Cd, i.e., $D_S = \phi^2 D$ where D is the self-diffusion coefficient of Cd in water at 4 °C (3.74×10^{-6} cm^2 s^{-1}; Li and Gregory, 1974); $d[Cd]/dx$ is the concentration gradient (mol cm^{-4}). Correction of D for the co-diffusion of other ions (Berner, 1980) was small (<1%) and thus was neglected. The values of J_D^{Cd} obtained with Eqn. 5 vary among sampling dates; for this reason, we calculated time-weighted average J values according to

Table 1. Estimated fluxes of cadmium across the sediment–water interface due to molecular diffusion, bioturbation and bioirrigation.

	Sept. 1997	Nov. 1997	May 1998	June 1998	July 1998	June 1999	Time-weighted average
J_D^{Cd} (10^{-11} mol cm^{-2} yr^{-1})	1.55	2.21	0.51	1.63	1.16	0.80	1.80
J_B^{Cd} (10^{-14} mol cm^{-2} yr^{-1})	0.90	1.28	0.29	0.94	0.67	0.46	1.04
J_I^{Cd} (10^{-11} mol cm^{-2} yr^{-1})	0.59	0	0.43	0.70	0.93	0.53	0.27
p (d)	50	217	26	15	43	15	

$$J = \frac{\Sigma J_i\, p_i}{\Sigma p_i}, \tag{6}$$

where p_i is the time period to which J_i applies. In this calculation, we assumed that the November 1997 [Cd]-depth profiles (Fig. 6b) apply for the period from October 1997 to early May 1998; the other p_i values were obtained by splitting days between sampling dates. Comparison, at a given sediment depth, of these time-weighted values of J_D^{Cd} with the apparent Cd accumulation rate in the sediments ($J_{app}^{Cd} = R_m \cdot \{Cd\}_T$) indicates that Cd redistribution in the solid phase should be negligible (<5%); we use the term "apparent" because the calculation does not consider post-depositional contributions (see Sect. 5.2.3). The above comparison of fluxes suggests that a significant remobilization of Cd from the solid phase and its redistribution within the sediment column is unlikely. However, definitive elimination of the possibility that these processes contribute to shaping the $\{Cd\}_T$-depth profile would require the direct measurement of the invertebrate diapause hypothesis (e.g., by deploying benthic chambers at various times of the year).

5.2.3. *Transport across the sediment–water interface by molecular diffusion, bioturbation, and bioirrigation*

Under steady state conditions, molecular diffusion, bioturbation, and irrigation can be taken into account by the one-dimensional mass conservation equation (Boudreau, 1997)

$$\frac{d}{dx}\left(\phi(D_S + D_B)\frac{d[Cd]}{dx}\right) + \phi\alpha([Cd]_{burrow} - [Cd]) + R = 0, \tag{7}$$

where $[Cd]_{burrow}$ and [Cd] are the aqueous concentrations of Cd in the burrow (assumed to be identical to that in the overlying water) and in the porewater, respectively; α is the bioirrigation coefficient (s^{-1}); and R is the rate of reaction of Cd (release to or fixation from porewater, depending on the sign; mole cm^{-3} s^{-1}). The contributions of advection and burial were neglected in Eqn. 7.

We have estimated the fluxes of dissolved Cd across the sediment–water interface due to molecular diffusion, bioturbation, and bioirrigation with the code PROFILE (Berg et al., 1998) which solves numerically Eqn. 7 to obtain values of R over depth intervals that yield the best fit of the modelled to the experimental [Cd]-depth profiles based on the least squares criterium. As input data to PROFILE, we used (i) the mean (n = 3) [Cd]-depth profiles shown in Figure 6 for each sampling date; the November 1997 and July 1998 profiles were shifted 1 cm upward to allow for the maximum [Cd] gradient to occur at the sediment–water interface; (ii) $D = 3.74 \times 10^{-6}$ cm^2 s^{-1} at 4 °C (Li and Gregory, 1974) and $\phi = 0.94$; (iii) $D_B = 2.2 \times 10^{-9}$ cm^2 s^{-1}, i.e., the largest value reported by Matisoff and Wang (2000) for chironomids (see Sect. 5.2.1); sediment particles and solution are mixed at the same rate by bioturbation, hence the same D_B value was used for solute as for particles. The bioirrigation coefficient α, which is required as input, was assumed to vary linearly from α^0 at the sediment surface to 0 at 10 cm (the maximum depth of occurrence of chironomids) and α^0 was calculated from (Boudreau, 1984)

$$\alpha^0 = \frac{D_s r_1}{(r_2^2 - r_1^2)(r_a - r_1)}, \tag{8}$$

where r_1 is the radius of an animal's tube, r_2 is half the distance between adjacent tubes if we assume that the tubes are uniformly distributed at the sediment surface, and r_a is the radial distance where the mean [Cd] occurs [taken here as $(r_1 + r_2)/2$]. Using $r_1 = 0.1$ cm and $r_2 = 1.5$ cm, we obtain $\alpha^0 = 2.6 \times 10^{-7}$ s^{-1}. Our estimated α^0 value agrees reasonably well with those measured by Matisoff and Wang (1998) for the chironomids *Coelotanypus* (6.3–9.5 $\times 10^{-7}$ s^{-1}) and *C. plumosus* (19.0×10^{-7} s^{-1}) if allowance is made for the fact that the density of animals was higher in their experimental setup than in L. Tantaré [as reported by Hare et al. (1994)]. The values of J_D, J_B, and J_I obtained on this basis vary among sampling dates (Table 1); we calculated time-weighted average J values with Eqn. 6 (Table 1).

Table 1 indicates that the estimated biodiffusional flux of Cd (J_B^{Cd}) is negligible compared to the flux due to molecular diffusion (J_D^{Cd}), an expected result, since D_B is much smaller than D_S. The estimated J_I^{Cd} represents probably a maximum value since we assumed a linear decrease of α with depth whereas an exponential decrease, which would lead to lower values of J_I^{Cd}, is more likely (Meile et al., 2001). Also, the value of $r_1 = 0.1$ cm assumed in the calculation of α^0 is probably an upper limit; smaller r_1 values would lead to smaller α^0 and J_I^{Cd} values. Finally, in the calculation of J_I^{Cd}, it is assumed that $[Cd]_{burrow}$, due to continuous irrigation of the burrows, is equal to [Cd] in the overlying water, which is an upper limit; lower $[Cd]_{burrow}$ would also lead to lower values of J_I^{Cd}.

5.2.4. *Flux of Cd deposited with settling particles*

Given that biological mixing of sediments is negligible, the net present-day deposition of Cd by settling particles (J_S^{Cd}) can be estimated as

$$J_S^{Cd} = R_m\{Cd\}_T, \tag{9}$$

where $\{Cd\}_T$ is the sediment Cd concentration in the top 0.5 cm interval. A value of $J_S^{Cd} = 3.3 \times 10^{-11}$ mol cm^{-2} yr^{-1} is

obtained. In this calculation, we assume that exchange of Cd between the solution and solid phase (e.g., mobilization or fixation) is negligible in the 0.5 cm sediment layer. This assumption is reasonable for several reasons. First, diffused Cd is fixed at about 1.5 cm, as suggested by the [Cd] gradients close to the sediment–water interface (Fig. 6). Indeed, if allowance is made for the precision on the measurement of [Cd] (coefficient of variation of 22%; see Sect. 3.2.2), most of the porewater [Cd] profiles show linear segments between 0.5 cm above and 1.5 cm below the sediment–water interface. Second, the porewater [Cd] profiles (Fig. 6) do not show any evidence of Cd remobilization in the 0–0.5 cm interval (perhaps with the exception of panel 6e), and calculations above (see Sect. 5.2.2) suggested that redistribution, to this sediment interval, of mobilized Cd is small. Third, the mean (±SD) concentration of Cd in settling particles collected in sediment traps deployed 2 m above the sediment surface on seven occasions during the ice-free period was 5.3 (±0.6) nmol g^{-1} (Alfaro–De la Torre, unpublished results); this concentration is similar to that measured in the 0.5 cm sediment layer (4.5 nmol g^{-1}).

5.2.5. *Historical changes in Cd fluxes*

The summation of our estimates of present-day J_S^{Cd} ($3.3 \pm 0.2 \times 10^{-11}$ mol cm^{-2} yr^{-1}), J_D^{Cd} ($1.8 \pm 0.3 \times 10^{-11}$ mol cm^{-2} yr^{-1}), J_B^{Cd} ($1.0 \pm 0.2 \times 10^{-14}$ mol cm^{-2} yr^{-1}), and J_I^{Cd} ($0.27 \pm 0.05 \times 10^{-11}$ mol cm^{-2} yr^{-1}) leads to a J_{acc}^{Cd} value of $5.4 \pm 0.4 \times 10^{-11}$ mol cm^{-2} yr^{-1} (Eqn. 3). The precision (±SD) indicated for the various fluxes has been calculated through propagation of errors by taking into account the precision of the concentrations and of the sediment accumulation rate. Based on these flux estimates, molecular diffusion, bioturbation, and bioirrigation represent at present about 33%, 0.02% and 5%, respectively, of total Cd accumulation in the sediment of L. Tantaré. High contributions of diffusion to sedimentary metal profiles, such as the one we estimated for Cd, have been reported for Zn in L. Tantaré and for Cu, Ni, and Zn in another acidic lake (L. Clearwater; Carignan and Nriagu, 1985; Carignan and Tessier, 1985).

Because of the postdepositional transfer of dissolved Cd across the sediment–water interface by molecular diffusion and benthic irrigation, the accumulation of Cd within a given sediment layer cannot be considered to be complete until this layer is buried below a depth of about 8 cm. Figure 3b shows how these two postdepositional transport processes will influence $\{Cd\}_T$ in each sediment layer as it passes below the zone influenced by these processes. In this simulation, we assumed (i) that the sedimentation rate will remain constant at its present-day value of 0.114 cm yr^{-1} for the next 70 years (i.e., the time required for the surficial layer of sediments to reach 8 cm depth), (ii) that bioirrigation and diffusion fluxes of Cd will remain constant at their present-day values (0.3×10^{-11} mol cm^{-2} yr^{-1} and 1.8×10^{-11} mol cm^{-2} yr^{-1}, respectively) for the time required for burial, (iii) that Cd diffusing across the sediment–water interface would be fixed only at 1.5 cm depth, (iv) that Cd bioirrigated across the interface will be evenly immobilized throughout the top 8 cm of the sediment column, and (v) that the processes of remobilization/redistribution of Cd in the sedimentary column are negligible. The simulation suggests that only the top 1.5 cm of the present $\{Cd\}_T$-depth profile should be modified significantly when the sediment is buried below 8 cm (Fig. 3b); the percentage increase in $\{Cd\}_T$ during this time period should be approximately 65%, 55%, 40%, and 2% for the 0–0.5 cm, 0.5–1.0 cm, 1.0–1.5 cm, and 1.5–2.0 cm intervals of the present-day sediment column, respectively. A similar increase in the vertical profile of J_{app}^{Cd} (Fig. 7) is expected if the sediment accumulation rate remains constant. The increase in $\{Cd\}_T$ (and J_{app}^{Cd}) after burial is due essentially to the diffusion of Cd across the sediment–water interface; the influence of bioirrigation is small. An important consequence of postdepositional accumulation of Cd is that it will be difficult to determine with great accuracy the input history of Cd from its sedimentary record in L. Tantaré.

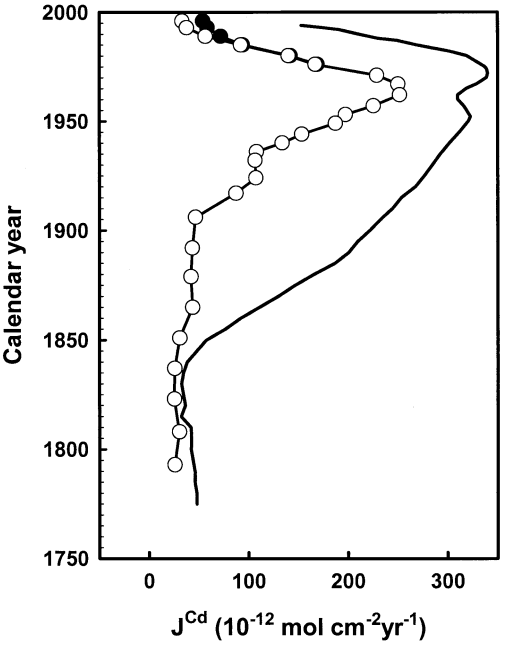

Fig. 7. Apparent accumulation (○) fluxes in L. Tantaré sediments as a function of calendar year; these fluxes are the product of R_m and $\{Cd\}_T$. Filled symbols indicate the expected fluxes when the sediment will be buried below 8 cm depth. The solid line without data points represents J^{Cd} ($\times 10^3$) in snowpacks from Greenland; it was calculated from Cd concentrations in snow given by Boutron (1995) multiplied by a constant mean annual snow accumulation rate of 21.5 g cm^{-2} yr^{-1} (Boutron et al., 1991).

The possibility that temporal changes in lake geochemistry affected Cd accumulation in the sediment column should also be considered. Indeed, there are indications from the present study that the L. Tantaré watershed has been subject to progressive acidification starting in about 1945 (see Sect. 5.1). Increased dissolved Cd concentrations due to watershed and lake acidification should lead to larger J_D^{Cd} and J_I^{Cd} fluxes across the sediment–water interface, lower J_S^{Cd}, and also to larger losses of Cd by lake outflow. Measurements of Cd adsorption onto settling particles collected with sediment traps from L. Tantaré showed that a decrease in pH from 6.5 to 5.5 increased dissolved Cd by 10–20% (Alfaro–De la Torre, unpublished results). This modest increase in lake [Cd] due to acidification could have affected slightly the shape of the accumulation rate profile of Cd. Acidification can also influence the transport of

sediments and metals within a lake. It promotes the growth of algal mats and plants that can change the sediment focussing process, which can in turn alter the deposition rate of sediments and metals at deep sites. Although the magnitude of this effect is difficult to evaluate, linearity in the log $^{210}Pb_{un}$ vs. depth plot (Fig. 2b) suggests that it was unimportant.

Figure 7 shows that the apparent accumulation fluxes of cadmium to the sediments of L. Tantaré are 1000× greater than those measured in Greenland ice (Boutron, 1995). The most plausible explanation for the much larger fluxes to lake sediments is a strong regional or continental component to atmospheric Cd. Stable Pb isotopes measurements in lichens (Carignan and Gariepy, 1995) suggest that the southern part of the Precambrian Shield, where L. Tantaré is located, receives most of its atmospheric Pb from U.S.A (60%) and Canadian (40%) sources (dominant winds are from the southwest); emissions of atmospheric Pb from metal smelters in northwestern Quebec were not detected. The Cd fluxes in L. Tantaré (Fig. 7) show a slow and progressive increase starting about 1879 followed by a sharper increase from about 1917 to 1967, and then a sharp decrease until 1995. As discussed above, these fluxes mainly reflect temporal change in the sedimentation and diffusion fluxes of Cd across the sediment–water interface rather than post-depositional remobilization/relocalization processes. We interpret the subsurface increase in Cd fluxes as being due to historical increases in atmospheric loading related to industrial activity and the incineration of municipal refuse, and the sharp decrease that follows as being due to the mitigation measures promulgated in Canada and the U.S.A. with respect to atmospheric emissions. The sharpness of these recent decreases is an indication that the mitigation measures have been very efficient.

6. CONCLUSIONS

Our sediment data present no evidence of biological mixing whereas porewater data present evidence of a postdepositional transport of Cd across the sediment–water interface by diffusion and bioirrigation and of Cd remobilization and redistribution in the sediment column. After considering critically the available data on sediments, porewater and macrobenthos, we conclude that the Cd flux profile in L. Tantaré has been produced more by variations in atmospheric Cd input than by diagenetic remobilization/redistribution processes. The relative insensitivity of the metal sediment profile to the activities of benthic organisms (bioturbation, bioirrigation) in L. Tantaré, likely results from the fact that this lake supports a rather sparse benthic community.

Acknowledgments—This study was supported by grants from the Natural Sciences and Engineering Research Council of Canada, the Ontario Power Generating Company, the Mining Association of Canada and the Fonds pour la Formation de Chercheurs et l'Aide à la Recherche. C.A. was supported by a fellowship from CONACYT–Mexico, Universidad Autónoma de San Luis Potosi–Mexico, and the Quebec Ministry of Education. We thank J.-C. Auclair, P. G. C. Campbell, R. Carignan, M. Courcelles, C. Gobeil, L. Hare, A. Mucci, S. Norton, T. Ouarda, and D. Rancourt for their comments, M. Courcelles for the dating measurements, L. Rancourt for technical assistance, and R. Rodrigue for his diving work. Permission from the Quebec Ministry of the Environment to work in the Tantaré Ecological Reserve is gratefully acknowledged.

Associate editor: A. Mucci

REFERENCES

Aller R. C. and Yingst J. Y. (1978) Biogeochemistry of tube-dwellings: A study of the sedentary polychaete *Amphitrite ornata* (Leidy). *J. Mar. Res.* **36,** 201–254.

Anderson R. F., Schiff S. L., and Hesslein R. H. (1987) Determining sediment accumulation and mixing rates using 210Pb, 137Cs, and other tracers: problems due to postdepositional mobility or coring artifacts. *Can. J. Fish. Aquat. Sci.* **44** (Suppl. 1), 231–250.

Appleby P. G., Richardson N., and Nolan P. J. (1991) 241Am dating of lake sediments. *Hydrobiologia* **214,** 35–42.

Berg P., Risgaard-Petersen N., and Rysgaard S. (1998) Interpretation of measured concentration profiles in sediment pore water. *Limnol. Oceanogr.* **43,** 1500–1510.

Berner R. A. (1980) *Early Diagenesis*. Princeton University Press.

Binford M. W. (1990) Calculation and uncertainty analysis of ^{210}Pb dates for PIRLA project lake sediment cores. *J. Paleolimnol.* **3,** 253–267.

Blais J. M., France R. L., Kimpe L. E., and Cornett R. J. (1998) Climatic changes in northwestern Ontario have had a greater effect on erosion and sediment accumulation than logging and fire: Evidence from 201Pb chronology in lake sediments. *Biogeochem.* **43,** 235–252.

Boudreau B. P. (1984) On the equivalence of nonlocal and radial-diffusion models for porewater irrigation. *J. Mar. Res.* **42,** 731–735.

Boudreau B. P. (1997) *Diagenetic Models and their Implementation*. Springer-Verlag.

Boutron C. F. (1995) Historical reconstruction of the earth's past atmospheric environment from Greenland and Antarctic snow and ice cores. *Environ. Rev.* **3,** 1–28.

Boutron C. F., Gorlach U., Candelone J. P., Bolshov M. A., and Delmas R. J. (1991) Decrease in anthropogenic lead, cadmium and zinc in Greenland snows since the late 1960s. *Nature* **353,** 153–156.

Buffle J. (1988) *Complexation Reactions in Aquatic Systems*. Ellis Horwood Ltd.

Carignan J. and Gariépy C. (1995) Isotopic composition of epiphytic lichens as a tracer of the sources of atmospheric lead emissions in southern Québec. *Geochim. Cosmochim. Acta* **59,** 4427–4433.

Carignan R. and Nriagu J. O. (1985) Trace metal deposition and mobility in the sediments of two lakes near Sudbury, Ontario. *Geochim. Cosmochim. Acta* **49,** 1753–1764.

Carignan R. and Tessier A. (1985) Zinc deposition in acid lakes: the role of diffusion. *Science* **228,** 1524–1526.

Carignan R., Rapin F., and Tessier A. (1985) Sediment porewater sampling for metal analysis: A comparison of techniques. *Geochim. Cosmochim. Acta* **49,** 2493–2497.

Carignan R., St-Pierre S., and Gächter R. (1994a) Use of diffusion samplers in oligotrophic lake sediments: Effects of free oxygen in sampler material. *Limnol. Oceanogr.* **39,** 468–474.

Carignan R., Lorrain S., and Lum K. A. (1994b) A 50-yr record of pollution by nutrients, trace metals, and organic chemicals in the St. Lawrence river. *Can. J. Fish. Aquat. Sci.* **51,** 1088–1100.

Cline J. D. (1969) Spectrophotomeric determination of hydrogen sulfide in natural waters. *Limnol. Oceanogr.* **14,** 454–458.

Coffman W. P. and Ferrington L. C. (1996) Chironomidae. In *An Introduction to the Aquatic Insects of North America* (ed. R. W. Merritt and K. W. Cummins), pp. 551–652. Kendall/Hunt.

Crusius J. and Anderson R. F. (1995) Sediment focusing in six small lakes inferred from radionuclide profiles. *J. Paleolimnol.* **13,** 143–155.

Davis R. B., Hess C. T., Norton S. A., Hanson D. W., Hoahland K. D., and Anderson D. S. (1984) 137Cs and 210Pb dating of sediments from soft-water lakes in New England (U.S.A.) and Scandinavia, a failure of 137Cs dating. *Chem. Geol.* **44,** 151–185.

Davison W. (1993) Iron and manganese in lakes. *Earth Sci. Rev.* **34,** 119–163.

Eakins J. and Morrison P. (1978) A new procedure for the determination of lead-210 in lake and marine sediments. *J. Appl. Radiat. Isot.* **29,** 532–536.

Edgington D. N. and Robbins J. A. (1976) Records of lead deposition in lake Michigan sediments since 1800. *Environ. Sci. Technol.* **10,** 266–274.

Eisenreich S. J., Metzer N. A., and Urban N. R. (1986) Response of atmospheric lead to decreased use of lead in gasoline. *Environ. Sci. Technol.* **20,** 171–174.

Evans H. E., Smith P. J., and Dillon P. J. (1983) Anthropogenic zinc and cadmium burdens in sediments of selected southern Ontario lakes. *Can. J. Fish. Aquat. Sci.* **40,** 570–579.

Fortin D., Leppard G. G., and Tessier A. (1993) Characteristics of lacustrine diagenetic iron oxyhydroxides. *Geochim. Cosmochim. Acta.* **57,** 4391–4404.

Gobeil C. (1999) Silver in sediments from the St. Lawrence River and Estuary and Saguenay Fjord. *Environ. Sci. Technol.* **33,** 2953–2957.

Gobeil C. and Cossa D. (1993) Mercury in sediments and sediment pore water in the Laurentian Trough. *Can. J. Fish. Aquat. Sci.* **50,** 1794–1800.

Gobeil C., Silverberg N., Sundby B., and Cossa D. (1987) Cadmium diagenesis in Laurentian Trough sediments. *Geochim. Cosmochim. Acta* **51,** 589–596.

Gobeil C., Macdonald R. W., and Smith J. N. (1999) Mercury profiles in sediments of the Arctic ocean basins. *Environ. Sci. Technol.* **33,** 4194–4198.

Guinasso N. L. and Schink D. R. (1975) Quantitative estimates of biological mixing rates in abyssal sediments. *J. Geophys. Res.* **80,** 3032–3043.

Hamilton-Taylor J., Willis M., and Reynold C. S. (1984) Depositional fluxes of metals and phytoplankton in Windermere as measured by sediment traps. *Limnol. Oceanogr.* **29,** 695–710.

Hare L., Carignan R., and Huerta-Diaz M. A. (1994) A field study of metal toxicity and accumulation by benthic invertebrates; implications for the acide-volatile sulfide (AVS) model. *Limnol. Oceanogr.* **39,** 1653–1668.

Heyvaert A. C., Reuter J. E., Slotton D. G., and Goldman C. R. (2000) Paleolimnological reconstruction of historical atmospheric lead and mercury deposition at Lake Tahoe, California–Nevada. *Environ. Sci. Technol.* **34,** 3588–3597.

Li Y.-H. and Gregory S. (1974) Diffusion of ions in sea water and in deep-sea sediments. *Geochim. Cosmochim. Acta* **38,** 703–714.

Martin C. W., Hornbeck J. W., Lickens G. E., and Buso D. C. (2000) Impacts of intensive harvesting on hydrology and nutrient dynamics of northern hardwood forests. *Can. J. Fish. Aquat. Sci.* **57** (Suppl. 2), 19–29.

Matisoff G. (1995) Effects of bioturbation on solute and particle transport in sediments. In *Metal Contaminated Aquatic Sediments* (ed. H. E. Allen), pp. 201–272. Ann Arbor Press.

Matisoff G. and Wang X. (1998) Solute transport in sediments by freshwater infaunal bioirrigators. *Limnol. Oceanogr.* **43,** 1487–1499.

Matisoff G. and Wang X. (2000) Particle mixing by freshwater infaunal bioirrigators: Midges (Chironomidae: Diptera) and mayflies (Ephemeridae: Ephemeroptera). *J. Great Lakes Res.* **26,** 174–182.

McCorkle D. C. and Klinkhammer G. P. (1991) Porewater cadmium geochemistry and the porewater cadmium: $\delta^{13}C$ relationship. *Geochim. Cosmochim. Acta* **55,** 161–168.

Meile C., Koretsky C. M., and Van Cappellen P. (2001) Quantifying bioirrigation in aquatic sediments: An inverse modeling approach. *Limnol. Oceanogr.* **46,** 164–177.

MEQ (1990) *Réserve écologique de Tantaré*. Ministère de l'Environnement du Québec, Direction du Patrimoine Écologique. Rapport No 3.19–64.

Morfett K., Davison W., and Hamilton-Taylor J. (1988) Trace metal dynamics in a seasonally anoxic lake. *Environ. Geol. Water Sci.* **11,** 107–114.

Norton S. A. and Kahl J. S. (1987) A comparison of lake sediments and ombrotrophic peat deposits as long-term monitors of atmospheric pollution. In *New Approaches to Monitoring Aquatic Ecosystems* (ed. T. P. Boyle), pp. 40–57. ASTM STP 940.

Norton S. A. and Kahl J. S. (1991) Progress in understanding the chemical stratigraphy of metals in lake sediments in relation to acidic precipitation. *Hydrobiologia* **214,** 77–84.

Norton S. A., Verta M., and Kahl J. S. (1991) Relative contributions to lake sediment chemistry by atmospheric deposition. *Verh. Internat. Verein. Limnol.* **24,** 2989–2993.

Nriagu J. O. (1990) The rise and fall of leaded gasoline. *Sci. Total Environ.* **92,** 13–28.

Nriagu J. O. and Rao S. S. (1987) Response of lake sediments to changes in trace metal emission from the smelters at Sudbury, Ontario. *Environ. Pollut.* **44,** 211–218.

Ouellet M. and Jones H. G. (1983) Paleolimnological evidence for the long-range atmospheric transport of acidic pollutants and heavy metals into the Province of Quebec, eastern Canada. *Can. J. Earth Sci.* **20,** 23–36.

Pacyna J. M., Scholtz M. T., and Li Y.-F. (1995) Global budget of trace metal sources. *Environ. Rev.* **3,** 145–159.

Pakarinen P., Tolonen K., Heikkinen S., and Nurmi A. (1983) Accumulation of metals in Finnish raised bogs. *Environ. Biogeochem. Ecol. Bull.* **35,** 377–382.

Payette S., Filion L., and Delwaide A. (1990) Disturbance regime of a cold temperate forest as deduced from tree-ring patterns: the Tantaré Ecological Reserve, Quebec. *Can. J. For. Res.* **20,** 1228–1241.

Powell D. E., Rada R. G., Wiener J. G., and Atchison G. J. (2000) Whole-lake burdens and spatial distribution of cadmium in sediments of Wisconsin seepage lakes, USA. *Environ. Toxicol. Chem.* **19,** 1523–1531.

Richardson G. M. (2000) *Critical Review on Natural Global/Regional Emissions of Metals to the Atmosphere*. O'Connor Associates Environmental Inc.

Robbins J. A. and Herche L. R. (1993) Models and uncertainty in 210Pb dating of sediments. *Verh. Internat. Verein. Limnol.* **25,** 217–222.

Robbins J. A. (1978) Geochemical and geophysical applications of radioactive lead. In *The Biogeochemistry of Lead in the Environment* (ed. J. O. Nriagu), pp. 285–393. Elsevier.

Sigg L., Sturm M., and Kistler D. (1987) Vertical transport of heavy metals by settling particles in Lake Zurich. *Limnol. Oceanogr.* **32,** 112–130.

SRC (1985) *Du plomb dans l'essence–Etude pour une politique au Canada: Rapport provisoire*. Report of the Royal Soceity of Canada.

Stumm W. and Morgan J. J. (1996) *Aquatic Chemistry*. 3rd ed. Wiley.

Tipping E. (1994) WHAM—A chemical equilibrium model and computer code for waters, sediments, and soils incorporating a discrete site/electrostatic model of ion-binding by humic substances. *Comp. Geosci.* **20,** 973–1023.

Tokeshi M. (1995) Life cycles and population dynamics. In *The Chironomidae* (eds. P. Armitage, P. S. Cranston, and L. C. V. Pinder), pp. 225–268. Chapman and Hall.

US EPA (1995) *National Air Pollutant Emission Trends, 1900–1994*. EPA-454/R-95-011. US Environmental Protection Agency, Washington, DC.

Wedepohl K. H. (1995) The composition of the continental crust. *Geochim. Cosmochim. Acta* **59,** 1217–1232.

Wong K. T., Nriagu J. O., and Coker R. D. (1984) Atmospheric input of heavy metals chronicled in lake sediments of the Algonquin Provincial Park, Ontario, Canada. *Chem. Geol.* **44,** 187–201.